Magnetic Resonance Image Post-Processing

for

Multiple Sclerosis Research

Mark A Horsfield, BSc, PhD, MIET, CEng

Medical Physics

Department of Cardiovascular Sciences

University of Leicester

Leicester Royal Infirmary

Leicester LE1 5WW

UK

Tel: +44-116-2585080

FAX: 44-116-2585979

e-mail: mah5@le.ac.uk

Running Title: MRI Post Processing

Key words: MRI, image analysis, post-processing, multiple sclerosis, visualization

Synopsis

Computerized image analysis is becoming more routine in multiple sclerosis research. This article reviews the common types of task that are performed when producing quantitative measures of disease status, progression or response to treatment. These tasks encompass uniformity (bias) correction; registration; segmentation; image algebra and fitting; diffusion tensor imaging and tractography; perfusion assessment; and 3-D visualization. The aim of these steps is to output reproducible, quantitative assessments of MRI scans that can be performed on data generated by the many different scanning sites that may be involved in multi-centre studies.

Introduction

Standard T_1- and T_2-weighting have formed the basis of contrast in most magnetic resonance (MR) images since the clinical utility of these types of scan was demonstrated by showing abnormal morphology or pathology (**Error! Reference source not found.Error! Reference source not found.Error! Reference source not found.**1, 2). For diagnostic purposes, a simple dual-echo T_2-weighted image will allow the radiologist or clinician to assess the number, position and shape of tissue abnormalities in the brain and spinal cord, all of which are factors in making a differential diagnoses of multiple sclerosis (MS). Lesions that enhance with injectable contrast agents such as gadolinium DTPA (Gd-DTPA) are most easily seen on T_1-weighted images (**Error! Reference source not found.**3).

However, the need to make quantitative measurements of factors that are more subtle, or open to subjective interpretation has long been recognized; for this, computerized analysis makes these sorts of measurement feasible or can assist in reducing any operator bias in the measurement, or even remove it completely. This review summarizes the tasks that are commonly applied in the analysis of MR images so that quantitative results can be presented.

Uniformity (Bias) Correction

MR images have an arbitrary intensity scale, where the actual intensity values depend on such factors as the receiver gain setting, as well as the sequence parameters (TR, TE) and tissue type. Furthermore, the intensity of a certain tissue type varies according to its position in the radio frequency (RF) transmitter and receiver coils, since the RF field and reception properties vary spatially. This

intensity non-uniformity (or bias) is most obvious in images acquired using surface receiver coils, such as those used for spinal cord imaging, but it is present in all MR scans (4**Error! Reference source not found.**).

For quantitative image analysis which relies on relative intensities, this bias is obviously a problem, and several methods for its correction have been put forward. Ideally, the bias field can be measured at the time of scanning by running extra pulse sequences, and then corrected *in situ*. However, retrospective correction has been investigated by a number of groups (see ref. 5**Error! Reference source not found.** for a review). A basic assumption behind all the retrospective correction methods is that the bias field varies only slowly in space which, given that the bias field comes mainly from non uniformities in the RF field, is a reasonable assumption. Some methods model the bias field as a sum of smooth polynomial or trigonometric functions (6,7), whilst others assume that bias field is (spatially) piecewise uniform (8). Other methods integrate the classification of tissue types (such as white matter, gray matter and CSF) with bias field correction by making the assumption that all tissues in the same class should have a similar intensity (9).

Accurate uniformity correction will become more important as the number of high-field scanners increases, and with the greater use of phased-array receiver coils for head imaging (Figure 1). Whatever the correction method, uniformity correction is used as a preprocessing step in a number of applications, particularly in image registration and segmentation.

Registration

Another common task that forms a part of many aspects of image analysis is

registration, where scans performed at different times are aligned so that the same anatomical locations can be superimposed (10). The time between scans may be of the order of a second or so, as is seen with fMRI where the registration corrects small amounts of patient movement. However, the time could be several years, in long-term follow-up studies of brain change. The scans may be performed with essentially the same type of contrast (for example, serial T_1-weighted images used to assess atrophy (11)), or they may have a different contrast or even be collected using a different imaging modalities (for example, to integrate data about glucose metabolism using positron emission tomography (PET) scans with high-resolution structural MRI scans (12)).

The process of registering images generally follows a common framework: by an iterative a process, a transform is calculated with distorts one scan (the 'floating image') so that it overlays another image (the 'base image') accurately. The parameters of the transform are adjusted to obtain a good match between the two images, and the goodness of the match is evaluated using a 'cost function'. The cost function is evaluated over the whole image (sometimes after background removal), and the choice of cost function is dictated by the types of image that are to be aligned. In cases where the images have very similar brightness and contrast (e.g., in fMRI time series), the root-mean-square difference or cross-correlation is most appropriate (13). Where images have similar contrast but different absolute intensity ranges (as can occur in images acquired with the same pulse sequence with a long time interval between acquisitions, or on different scanners) then the standard deviation of the intensity ratio can be useful (14).

Where images are acquired with different contrast or with different modalities,

another class of cost function should be used. These rely on the assumption that although the intensities at the same anatomical location may not be similar across modalities, the intensities are consistent such that a certain tissue type will have a fairly constant intensity for any one modality. When the two images are closely aligned, a two-dimensional (joint) histogram of intensities formed from the images will therefore show sharp peaks, and any mis-alignment will cause a blurring of the histogram because tissues of different types will overlap. Woods and mutual information are amongst these types of cost function, and they are a measure of this blurring of the joint histogram (15).

In order to compare images from different patients, it is necessary to transform them into a standard, anatomical space. One such space is based on the MNI brain atlas from the Montreal Neurological Institute. This was composed by registering the scans from a large sample of control subjects to an average brain that was previously created by transforming a large number of other scans to the standard space of Talairach and Tournoux (13). The original Talairach atlas (16) was created from a single, rather unrepresentative subject *post mortem*, which has resulted in some differences between the MNI atlas and the Talairach atlas. Nevertheless, for the purposes of identifying gross anatomical features, the MNI atlas serves well, and the disparity can largely be corrected by applying an additional transform (17). Therefore, after registering a set of scans to the MNI atlas, it is possible to compare image features between subjects, in anatomical space.

One use of this type of registration to standard space is so-called voxel-based morphometry (VBM) analysis, such as that built into the Statistical Parametric Mapping (SPM) package from the Wellcome Trust Centre for Neuroimaging, London

(18). The goal of VBM is to allow the identification of significant differences in brain tissue between groups of subjects, and it allows the regional and anatomical variation to be visualized (19), revealing the subtle changes that can occur, and the differences between the different MS phenotypes.

Most registration is done using a simple distortion to transform the image to be registered, such as the affine transform, a property of which is that it always preserves the straightness of straight lines when the transform is applied. This type of linear transform cannot therefore account for the complex differences in the shapes of the brain that occur between individuals; more complex general transforms are needed in this case. Registration using non-linear transforms is now becoming a much more mature procedure, although it it still very compute intensive. The deformation required to bring about registration is normally modeled as a sum a polynomial, trigonometric or radially-symmetric basis functions (20). It is used for inter-subject registration or for assessing atrophy within a subject (21). Figure 2 shows an attempt to register an MS patient with a severely atrophied brain to a control subject, first using a simple affine transform, and then with non-linear registration using radial basis functions to model the deformation field (20). Considering the severity of the atrophy, the non-linear registration produces quite a good anatomical match between the patient and control.

Image Segmentation

Image segmentation refers to the process of splitting an image into multiple regions (sets of pixels). Segmentation of MRI scans is typically used to identify different types of tissue, and their boundaries, so that the volumes or shapes of the

individual tissues can be quantified or analysed further.

Image segmentation can result in either a set of regions that, when combined, cover the entire image, or a set of object boundaries such that each of the pixels in a region has some similarity to the others in that object. The similarity may be a simple intensity similarity, or contain information about connectivity within a regions, or be based on some collective shape property. The objective is usually to determine regions that form a set of tissue types such as white-matter, gray-matter or MS lesion.

Measurement of Lesion Volumes

Probably the first and most straightforward use of segmentation in the field of MS research was to determine the volume of hyperintense lesions on T_2-weighted images. The segmentation of MS lesions can be done by manually drawing around the boundary of the lesions whilst showing the scans slice-by-slice on a computer display. Using this process, it is quite possible to achieve reasonable reproducibility, but it is very labour intensive. Changes in lesion volumes are used as secondary outcomes measures in clinical trials of new putative treatments for MS, and the lesions may be hyperintense (22) on T_2-weighted images, or hypointense on T_1-weighted images ('black holes') (23). Black hole lesions are thought to represent tissues with more severe cellular damage (24).

Many workers have addressed the problem of reducing the amount of operator time and improving the reproducibility of the measurement of MS lesion volumes using computer-assisted or fully-automated computerized methods. Methods include edge detection and contour following (25,26), multi-parametric

image analysis (27,28,29), template-driven segmentation (31,32) and fuzzy connectedness (33). Of these, probably the one which is most commonly-used in clinical trials is one which still relies on operator judgement to identify the individual lesions, but which uses an edge detector to find the border of the lesion (26). The operator visually determines a fairly well-defined portion of the lesion boundary and clicks on it with the computer mouse; an edge detector selects the sharpest part of the boundary and a contour surrounding the lesion is generated by following a level of iso-intensity from the initial edge point. This simple method has been shown to considerably improve reproducibility compared to manual outlining (25).

Many other methods are used by individual research groups for their own clinical and MRI research programmes. The reproducibilities are often shown to be better than manual identification and outlining, but they are often tested using data from only one MRI scanner with specific pulse sequence parameters. It may be that some of these methods do not transfer to the context of multi-centre clinical trials because they are sensitive to the subtle differences in images seen between different manufacturers for what are nominally the same pulse sequence parameters.

Probably the most promising approaches are based on multi-parametric segmentation, where information from a number of scans (such as the two echoes of a dual-echo sequence, and FLAIR) are combined to segment the lesions based on the position of pixels in an *N*-dimensional intensity space (34). The number of dimensions is equal to the number of images and, in principle, the greater the number of images used, the higher will be the discriminating power that will allow lesion to be distinguished from other tissues. Fuzzy connectedness can be regarded

as an extension of multi-parametric methods, but it is a general method for image segmentation in which the object membership of pixels depends on the way they "hang together" spatially in spite of gradual variations in their intensity. For the task of measuring lesion volumes, Udupa et al. (33)**Error! Reference source not found.** adopted a three-part procedure: first was the manual identification by the operator of a few typical tissue types on the scan: MS lesion, normal white matter, normal gray matter, and CSF. Next, the fuzzy connectedness algorithm automatically identified "candidate" MS lesions, and in the final stage these candidates lesions were presented to the operator who reviewed them and accepted, rejected or modified them. Thus, the method implicitly recognized that human operators are good at identifying image features, but do not perform well when attempting to delineate the poorly-defined borders of the lesions. The operator time required to assess typical image sets from MS patients was between 2 and 20 minutes, depending on the number and complexity of the lesions. Another approach based on fuzzy connectedness principles incorporated "domain knowledge" in the form of probability maps, which showed the probability of finding MS lesion tissue at any given anatomical location (35). This allowed the number of "false positive" lesions to be greatly reduced, eliminating the need for review. However, it was still necessary for the operator to manually identify each MS lesion with a mouse click.

Atrophy

Brain and spinal cord atrophy measures are becoming standard in MS clinical trials, where the loss of neuronal tissue is thought to be an indicator of long-term irreversible tissue damage (36). This is slightly complicated by the phenomenon of 'pseudo atrophy' where by the anti-inflammatory effect of some treatments causes a

rapid initial loss of brain volume because of a reduction in the amount of excess fluid in the brain. Brain atrophy is a normal feature of ageing, with progressive loss of tissue starting in early adulthood (37). However, the brain volume is highly variable amongst individuals.

Brain atrophy can be measured either cross-sectionally or longitudinally. Cross-sectional measures estimate the total volume of brain tissue. However, since the cranial volume and brain size are so variable, the results are not easily compared except in studies of very large populations. One way to standardize the measures is to provide a 'normalized' brain volume, and there are really two ways to do this. The first is to divide the brain parenchymal volume by the cranial volume, since the cranial volume remains largely fixed throughout adult life (38). The second is to divide it by the sum of the parenchymal and CSF volumes to form what is known as the brain parenchymal fraction (BPF) (39). As atrophy occurs, the CSF-filled ventricles and sulci enlarge and the BPF reduces, and therefore the BPF is a highly-effective measure of the state of atrophy which can be compared across individuals. In longitudinal studies, it is of course possible simply to measure the reduction in normalized brain volume over time. However, more sophisticated approaches first register the scans made at different time points; it then becomes possible not only to assess the gross change in tissue volume, but also to visualize the anatomical location of tissue loss (40).

While there are several software packages that can be used to assess atrophy, it is necessary that they have a scan-rescan coefficient of variation of around 0.5% or better if they are to be useful for MS research. This allows differences in atrophy rates between groups of subjects to be assessed with

relatively small groups (typically 25-50) (41). Virtually all methods use high-resolution T_1-weighted images (either multi-slice spin-echo or 3-D gradient-echo) as input, where the timing parameters are optimised to maximise contrast between the low-intensity CSF and the parenchyma. As a pre-processing step, it is necessary to separate the cranial contents from other tissues such as scalp, eyes and facial tissues; this can be achieved in a variety of ways, but one of the most popular is the Brain Extraction Tool (42), which uses an expanding triangulated surface model which "sticks" to the brain/CSF boundary as it expands from the centre of the brain. With sufficient image contrast, segmentation can then be achieved using an intensity threshold to separate brain from CSF (39). More sophisticated approaches assess gray matter, white matter and CSF volumes separately, allowing loss of different types of tissue to be assessed (37); however, this method is prone to errors due to the misclassification of MS lesions as gray matter. Taking this a stage further, a VBM approach allows the identification of the individual brain structures that are particularly subject to atrophy (19).

It has also been shown that the spinal cord is subject to atrophy, and that the degree of atrophy is related to disability (43). The cord is of course a much smaller structure and, because of this, cord atrophy measurements have a much lower reproducibility (larger CoV) than those for the whole brain. A typical approach is to measure the cord area over a fairly limited portion of the cervical region. The cord can be segmented using methods similar to those used in the brain, either with a threshold to separate to CSF from the cord parenchyma (44), or using edge detection (43).

Magnetization Transfer

Standard MRI detects signal only from hydrogen nuclei (protons) that are "mobile" (contained within a liquid)—if a hydrogen atom is part of a molecule that is large and cannot move about freely, then the signal from that hydrogen atom will decay too quickly to be seen using a clinical MRI scanner. Such protons are found in large molecules (macromolecules) such as large proteins, cell membranes, and myelin. However, the mobile protons are in constant motion and come into regular and intimate contact with the macromolecular protons, and the spin state (the proton magnetization state, which is measured with MRI) of the mobile protons can exchange with that of the macromolecular protons. This exchange of magnetization forms the basis of magnetization transfer imaging (MTI) (45).

A magnetization transfer ratio (MTR) image is calculated from a pair of images acquired in an identical way, except that one has extra off-resonance RF pulses applied, which saturate the macromolecular magnetization pool. The MTR is calculated for every corresponding pair of pixels in the two images. If the intensity of the pixel in the image without saturation pulses is M_0, and the corresponding intensity in the image with saturation pulses is M_s, then the MTR is:

$$\mathrm{MTR} = \frac{\left[M_0 - M_s\right]}{M_0}.100\% \ .$$

The application of formulae such as the one above, on a pixel-by-pixel basis is a straightforward procedure of image processing, and is generally referred to as "image algebra".

Misregistration can occur if the subject moves between the two scans, but the

M_0 and M_s images must be in register, otherwise artifacts will appear at the edges of features in the calculated MTR image, with false MTR values. It is best to acquire the two images in an interleaved way (46,47), although it is possible to register them after acquisition.

Two forms of data analysis have been used extensively for MTR images: region of interest and histogram analysis. Region of interest (ROI) analysis may be useful for elucidating the degree of tissue damage within individual lesions seen on T_2-weighted scans, or within anatomical regions associated with particular symptoms. ROI analysis, however, can be subject to operator bias because the placement of regions is normally done manually. This could be overcome by first registering scans to an anatomical template and using ROIs defined on the template image. With MTR histogram analysis, a histogram of pixel MTR values is formed from the whole of the brain parenchyma; thus, both focal damage and more widespread diffuse tissue damage are reflected in changes to the shape of the histogram, with a general shift towards lower MTR values as the density of macromolecules is reduced with demyelination or axonal loss. Extraction of the brain parenchyma, using the same procedures that are used in atrophy measurements is a necessary pre-processing step. After normalization (to remove any effect of the absolute brain size) the MTR histogram can be characterised by a number of simple statistics such as the histogram peak position, the peak height and the average MTR.

Least-Squares Fitting and Relaxometry

The calculated MTR images noted in the previous section allow a quantitative

approach to the assessment of tissue damage. Whilst T_1- and T_2-weighted images show, qualitatively, the burden of tissue damaged by MS, a quantitative approach to relaxation time measurements is more rigorous. The mapping of T_1, T_2 and T_2* (or their inverses R_1, R_2 and R_2*) is possible if images are acquired with more than one set of timing parameters: T_1 maps can be produced from a series of images with varying TR, inversion time (TI) or flip angle (for gradient-echo sequences) (48); T_2 maps from spin-echo images and T_2* images from gradient-echo images with varying echo times (49).

In a way that is similar to pixel-by-pixel MTR calculation, the relaxation time constants are calculated for every image pixel, normally by least-squares fitting to the different images. At least two images are needed to estimate simple T_1 or T_2 maps, since the fitted variables include the proton density as well as the relaxation time: the number of images acquired must be at least as many as the number of fit variables. Increasing the number of acquired images reduces the sensitivity to noise, reducing errors in the estimates of the fit variables. Figure 3 shows relaxation time and rate maps created from data collected using a dual-spin-echo sequence (T_2) and a sixteen-echo gradient-echo sequence (T_2*).

Simple least-squares fitting can reliably fit a single exponential decay curve, and possibly even a couple of isolated exponential components (50). However, because of noise in the data, fitting multiple relaxation components, representing different tissue water components, is notoriously unreliable. To make fitting stable, it is common to “regularize” the fitting procedure by fitting a smooth distribution of exponential components (51). This approach has been taken by the group of MacKay in Vancouver, to produce T_2 distributions from brain tissue (52). Three

peaks in the white matter T_2 distribution are attributed to: water between the myelin lipid bilayers (T_2 between 10 and 50 ms); intracellular water (T_2 of approximately 70 ms); and CSF (T_2 > 1 second) (Figure 4). In recent studies, maps of the short T_2 component have been shown to correlate strongly with myelin staining in *post-mortem* samples (53) (Figure 5).

Diffusion Tensor Imaging

Diffusion-weighted (DW) MR imaging has been used in the human brain for almost 20 years, to investigate numerous conditions, including multiple sclerosis (MS) (54,55). The contrast in DW MRI is based on the diffusional displacement of water molecules which, in the presence of a strong magnetic field gradient, causes the signal intensity to be attenuated. In simple anisotropic systems, diffusion in three dimensions can be represented mathematically by the diffusion tensor, a 3×3 matrix which specifies the root mean square diffusional displacements in any direction (56). It is common to display images of properties of tensor, rather than the tensor its self (see Figure 6).

Echo planar imaging (57) is normally used for diffusion-weighted applications because of the technique's insensitivity to bulk patient motion. However, because of scanner hardware limitations, diffusion-weighting gradient pulses usually induce some distortions in DW EPI images, characterized by a shear, shift and scaling of the images in the phase-encoded direction. The post-processing correction of these distortions has been subject to a good deal of work; the most successful methods exploit the relationship between the type and magnitude of distortion and the magnetic field gradient vector direction and amplitude (58,59). One approach is also

capable of including a model of patient motion, so that gradient-induced distortion and patient motion can be corrected simultaneously (60).

After distortion correction, calculation of the tensor is relatively straightforward problem in multivariate regression (56). Diagonalization of the tensor to extract the principal axes allows images showing the direction of greatest diffusivity, the degree of anisotropy, and the directionally-averaged diffusivity (mean diffusivity, equivalent to one third of the Trace of the diffusion tensor) to be synthesized (Figure 6). All these properties of the tensor reflect the diffusional behavior of water in the tissue and, given similar acquisition parameters, should be comparable across sites and at different field strengths.

Once the tensor is computed, it is possible to reconstruct the spatial path of the major white matter axonal bundles in 'fibre tracking' applications (61). Tractography is performed by following the direction of largest diffusivity to reconstruct a pathway corresponding to the underlying axonal fibre bundle. This allows the study of human white matter anatomy that could previously only be accessed by *post mortem* dissection. Tissue damage along the reconstructed tracts can then be assessed by evaluating other parameters, such as the fractional anisotropy or mean diffusivity, along the tract (62,63).

One problem with performing tractography on MS patients is that diffusion anisotropy is reduced in MS lesions, and a reduction in anisotropy leads to a greater uncertainty in the estimated principal diffusion direction (64) (see Figure 6 and Figure 7). Tracking through lesions is therefore problematic, and it may be necessary to use an 'atlas-based' approach to determining the tissue characteristics within specific tracts, having first localized the tracts by performing fiber tracking on a large

population (65).

The simple model of diffusion that is provided by the diffusion tensor cannot capture the details of diffusion in complex white matter regions; these occur in brain areas where fibers merge and cross. MRI does not have the spatial resolution to resolve the individual fiber bundles, but the MRI methods are sensitive to the diffusion of water over distances of a few microns; detailed analysis of the diffusion behavior can reveal more about white matter architecture on a smaller scale where an individual image voxel contains a mixed population of fibers. Approaches such as q-ball imaging (66) and determining the fiber orientation density function (ODF) (67) can resolve more details about these regions of mixed fiber orientations.

Perfusion

Abnormalities of cerebral blood flow (CBF) have long been recognised in MS, and MRI can be used to assess perfusion *in vivo*. Perfusion can be measured in either of two ways: using standard injectable MRI contrast agents as a bolus (bolus tracking), or by using blood as an endogenous contrast agent, an experiment that is known as arterial spin labelling (ASL).

For bolus tracking, images are acquired rapidly and continuously as the contrast agent is injected over a short time (normally around five seconds) into the antecubital vein. From there, the bolus is carried to the heart, through the lungs, back to the heart and then to the arterial system where it can be measured in the carotid arteries, circle of Willis, or the cerebral arteries. The images are normally acquired using an echo-planar sequence to give good time resolution (of the order of one or two seconds) and to give a large signal reduction as the contrast agent

passes through. This signal reduction is used to estimate the concentration of contrast agent for every voxel from the relaxivity and echo time of the sequence.

By the time the contrast agent arrives in the feeding arteries, considerable dispersion has occurred, and the arterial input into the brain is no longer a short, sharp bolus as would be required for straightforward analysis. An important part of the processing of bolus tracking data is therefore to account for this dispersion, by a process of "deconvolution" (68). This mathematical process examines the real dispersed contrast agent input and the real passage through the brain tissue, and reconstitutes what would have been the response to an ideal sharp "impulse" of contrast agent. This reconstructed impulse response is used to calculate the mean transit time (MTT) for contrast passage, and the cerebral blood volume (CBV) can be assessed by measuring the degree of signal change in the brain tissue compared to that in an artery. The cerebral blood flow can then be calculated from the ratio:

$$\mathrm{CBF} = \frac{\mathrm{CBV}}{\mathrm{MTT}} \ .$$

Bolus tracking experiments are not normally considered to give accurate quantitative CBF values, mainly because of the difficulty of obtaining accurate estimates of the contrast agent concentration in the arteries and in the capillary bed: the relaxivity in T_2- and T_2*-weighted pulses sequences depends on the size of the vessels that contain the blood. Furthermore, estimation depends on the contrast agent remaining within the vessels, and where disease is present, the blood-brain-barrier may not be intact and the contrast agent leaks into tissue; however, it is possible to correct for this (69). In spite of these problems, bolus tracking is considered to give good qualitative CBF maps, which can be used to make relative

comparisons across regions within a single patient.

The basic idea of arterial spin labeling is to acquire two images: in the first, the blood is “labeled” before it moves into the imaged slice, usually by inverting the magnetization; the second is a control image in which no labeling takes place. If carefully performed, the difference between the two images is then solely due to the labeled blood that has perfused the tissue volume imaged. However, since the brain blood volume fraction is small, the signal difference is also very small (of the order of 1%), and so this technique has inherently poor SNR. Acquisition over a long period, with signal averaging, is usually necessary, and the method is of most use at higher field strength. The advantage of ASL over bolus tracking methods is that repeated measures can be made, and the response to various interventions monitored as long as changes in blood flow occur and can be sustained over time scales longer than the acquisition time for a single measurement (typically 5 minutes). It is also totally non-invasive since no contrast agent injection is needed.

There are many variants of the ASL experiment, which are designed to permit more complex assessment of the confounding factors that inhibit quantitative measurement of perfusion. One of the most common variants introduces a variable transit time between the inversion and the image readout in the brain; the impact of variable transit times then be taken into account (70). The details of processing of ASL data depend, of course, on the exact form of experiment, and vary in complexity from a simple subtraction to a least-squares fitting to extract the various model parameters, including CBF; see (71) for a review.

Both bolus tracking (72) and ASL (73) methods have been used to map the regional changes in blood flow that develop with MS, with reduced perfusion being

seen in both white and gray matter. Correlations have been seen between white matter perfusion and disability (72), and between gray matter perfusion and neuropsychological impairment (74).

Visualization

The mainstay of MR image computerized visualization is still the common multi-slice viewing system, analogous to a conventional light box, where image slices can be viewed either singly, with arrays of slices, and preferably with images of different contrast being viewable side-by-side. For manual analysis (such as counting the numbers of lesions), semi-automated analysis (semi-automatically outlining lesions (26)), or reviewing the output of fully-automated methods (75), this sort of presentation tool is very efficient, enabling rapid throughput.

However, 3-dimensional visualization tools are popular for data exploration and presentation (77,78). These generally allow surface models and cut-planes to be viewed simultaneously, so that the spatial relationships between the various anatomical elements can be better appreciated (Figure 8). Whilst these tools are established as valuable aids in other medical settings, such as surgical planning (79), they are difficult to integrate into quantitative analysis procedures for MS research, in a useful way.

Data handling

In the context of multi-centre clinical trials, central analysis of image data is essential for improving the quality of data acquisition, consistency of processing, achieving validation of processing methods, and data archiving to the standards required for clinical trials of new therapeutic agents (80). Basic transfer of image data

has been greatly facilitated in the last few years by the adoption of the Digital Imaging and Communication in Medicine (DICOM) standards for image exchange by all mainstream manufacturers of medical equipment (81). This allows data to be sent for analysis either by fairly conventional means (by sending an archive CD-ROM in the mail) or by transfer using standard methods over the Internet.

Having received the image data, some groups have adopted a “pipeline” processing approach to ensure efficiency, consistency, and quality control of the analysis procedure (75,76). By integrating the analysis pipeline with a database of patients enrolled in a trial and the trial scanning schedules, quality can be improved and the tasks streamlined. The sorts of task that can be automated by the pipeline include sending out automatic reminders to participating sites about scans which are due or not received; automatically implementing pre- and post-processing steps; prioritizing and presenting tasks to be performed by neurologists, technologists and technicians; generating and collating reports; and archive of data.

Concluding Remarks

Image analysis methods have become much more mainstream over the last five years or so, and there are now many excellent tools available to enable the non-specialist to participate in the sorts of task that were once considered to be only for those with expert knowledge and large computing resources. The resources required were not only specialist and expensive computer equipment, but also technical personnel who would implement and integrate the necessary processing steps. With the advent of very powerful and inexpensive personal computers, and mature software applications that have been designed for the general user, post-processing

of MRI data for quantitative analysis of MS patients' scans is becoming much more mainstream. Over time, I expect that some of these methods will become integrated into routine clinical practice so that, for example, individual patients' disease progression can be monitored, and treatment plans designed accordingly.

References

1. Bydder GM, Steiner RE, Young IR, et al. Clinical NMR imaging of the brain: 140 cases. AJR 1982;139(2):215-236.

2. Rinck PA, Bielke G, Meves M. Modified spin-echo sequence in tumor diagnosis. Proceedings. The Society of Magnetic Resonance in Medicine. Second Annual Meeting. San Francisco 1983. 300-301.

3. Miller DH, Rudge P, Johnson G, et al. Serial gadolinium enhanced magnetic-resonance imaging in multiple sclerosis. Brain 1988;111(4):927-939.

4. Wicks DAG, Barker GJ, Tofts PS. Correction of intensity nonuniformity in MR images of any orientation. Magn Reson Imag 1993;11(2): 183-196.

5. Belaroussi B, Milles J, Carme S, et al. Intensity non-uniformity correction in MRI: existing methods and their validation. Med Image Anal 2006;10(2): 234-246.

6. Horsfield MA, Rovaris M, Rocca MA, Rossi P, Benedict RH, Filippi M, Bakshi R. Whole-brain atrophy in multiple sclerosis measured by two segmentation processes from various MRI sequences. J Neurol Sci 2003;216(1):169-77.

7. Brechbuhler C, Gerig G, Szekely. Compensation of spatial inhomogeneity in MRI based on a parametric bias estimate. Visualization in Biomedical Computing 1996;1131:141-146.

8. Sled JG, Zijdenbos AP, Evans AC. A nonparametric method for automatic correction of intensity nonuniformity in MRI data. IEEE Trans Med Imaging 1998;17(1):87-97.

9. Gispert JD, Reig S, Pascau J, et al. Method for bias field correction of brain T1-weighted magnetic resonance images minimizing segmentation error. Hum Brain

Mapp 2004;22(2):133-144.

10. Hill DLG, Batchelor PG, Holden M, et al. Medical image registration. Phys Med Biol 2001;46(3):R1-R45.

11. Fox NC, Freeborough PA. Brain atrophy progression measured from registered serial MRI: Validation and application to Alzheimer's disease. JMRI 1997;7(6):1069-1075.

12. Studholme C, Hill DLG, Hawkes DJ. Automated three-dimensional registration of magnetic resonance and positron emission tomography brain images by multiresolution optimization of voxel similarity measures. Med Phys 1997;24(1):25-35.

13. Collins DL, Neelin P, Peters TM, et al. Automatic 3D intersubject registration of MR volumetric data in standardized Talairach space. J Comput Assist Tomogr 1994;18(2):192-205.

14. Woods RP, Grafton ST, Holmes CJ, et al. Automated image registration: I. General methods and intrasubject, intramodality validation. J Comput Assist Tomogr 1998;22(1):139-152.

15. Pluim JPW, Maintz JBA, Viergever MA. Mutual-information-based registration of medical images: a survey. IEEE Trans Med Imaging 2003;22(8)986-1004.

16. Talairach J, Tournoux P. (1988): Co-Planar Stereotaxic Atlas of the human brain. New York: Thieme Medical Publishers.

17. Lancaster JL, Tordesillas-Gutierrez D, Martinez M, et al. Bias between MNI and talairach coordinates analyzed using the ICBM-152 brain template. Hum Brain Mapp 2007;28(11):1194-1205.

18 . Mechelli A, Price CJ, Friston KJ, et al. Voxel-based morphometry of the human

brain: methods and applications. Current Medical Imaging Reviews 2005;1(2):105-113.

19. Sepulcre J, Sastre-Garriga J, Cercignani M, et al. Regional gray matter atrophy in early primary progressive multiple sclerosis - a voxel-based morphometry study. Arch Neurol 2006;63(8):1175-1180.

20. Rohde G, GK, Aldroubi A, Dawant BM. The adaptive bases algorithm for intensity-based nonrigid image registration. IEEE Trans Med Imaging. 2003;22(11):1470-1479.

21. Pagani E, Horsfield MA, Rocca MA, Filippi M. Assessing atrophy of the major white matter fiber bundles of the brain from diffusion tensor MRI data. Magn Reson Med 2007;58(3):527-34.

22. Filippi M, Horsfield MA, Ader HJ, et al. Guidelines for using quantitative measures of brain magnetic resonance imaging abnormalities in monitoring the treatment of multiple sclerosis. Ann Neurol 1998;43(4):499-506.

23. Tomassini V, Paolillo A, Russo P, et al. Predictors of long-term clinical response to interferon beta therapy in relapsing multiple sclerosis. J Neurol 2006;253(3):287-293.

24. Barkhof F, Karas GB, van Walderveen MAA. T1 hypointensities and axonal loss. Neuroimaging Clin North Am 2000;10(4):739-752.

25. Grimaud J, Lai M, Thorpe J, et al., Quantification of MRI lesion load in multiple sclerosis: a comparison of three computer-assisted techniques. Magn Reson Imaging 1996;14(5):495-505.

26. Cader S, Cifelli A, Abu-Omar Y, et al. Reduced brain functional reserve and altered functional connectivity in patients with multiple sclerosis. Brain

2006;129(2):527-537.

27. Kikinis R, Shenton ME, Gerig G, et al. Routine quantitative analysis of brain and cerebrospinal fluid spaces with MR imaging. JMRI 1992;2(2):619-629.

28. Bedell BJ, Narayana PA, Wolinsky JS. A dual approach for minimizing false lesion classifications on magnetic resonance images. Magn Reson Med 1997;37(1):94-102.

29. Zijdenbos A, Forghani R, Evans A. Automatic quantification of MS lesions in 3D MRI brain data sets: validation of INSECT. Lecture Notes in Computer Science 1998;1496:439-448.

30. P. Anbeek KL, Vincken KL, van Osch MJP, et al. Probabilistic segmentation of white lesions in MR imaging. Neuroimage 2004;21(3):1037-1044.

31 . van Leemput K, Maes F, Vandermeulen D, et al. Automated segmentation of multiple sclerosis lesions by model outlier detection. IEEE Trans Med Imaging 2001;20(8):677-688.

32. Warfield S, Dengler J, Zaers J, et al. Automatic identification of gray matter structures from MRI to improve the segmentation of white matter lesions. J Image Guid Surg 1995;1(6):326-338.

33 . Udupa JK, Wei L, Samarasekera S, et al. Multiple sclerosis lesion quantification using fuzzy-connectedness principles. IEEE Trans Med Imaging 1997;16():598-609.

34. Sajja BR, Datta S, He RJ, et al. Unified approach for multiple sclerosis lesion segmentation on brain MRI. Ann Biomed Eng 2006;442(1):142-151.

35. Horsfield MA, Bakshi R, Rovaris M, et al. Incorporating domain knowledge into the fuzzy connectedness framework: Application to brain lesion volume estimation in multiple sclerosis. IEEE Trans Med Imaging 2007;26(12):1670-1680.

36. Fisher E, Rudick RA, Simon JH, et al. Eight-year follow-up study of brain atrophy in patients with MS. Neurology 2002;59(9):1412-1420.

37. Good CD, Johnsrude IS, Ashburner J, et al. A voxel-based morphometric study of ageing in 465 normal adult human brains. Neuroimage 2001;14(1):21-36.

38. Smith SM, Zhang YY, Jenkinson M, et al. Accurate, robust, and automated longitudinal and cross-sectional brain change analysis. Neuroimage 2002;17(1):479-489.

39. Rudick RA, Fisher E, Lee JC, et al. Use of the brain parenchymal fraction to measure whole brain atrophy in relapsing-remitting MS. Neurology 1999;53(8):1698-1704.

40 . Freeborough PA, Fox NC. Modeling brain deformations in Alzheimer disease by fluid registration of serial 3D MR images. J Comput Assist Tomogr 1998;22(5)838-843.

41. Fox NC, Jenkins R, Leary SM, et al. Progressive cerebral atrophy in MS - a serial study using registered, volumetric MRI. Neurology 2000;54(4):807-812.

42. Smith SM. Fast robust automated brain extraction. Hum Brain Mapp 2002;17(3):143-155.

43. Lin X, Tench CR, Turner B, et al. Spinal cord atrophy and disability in multiple sclerosis over four years: application of a reproducible automated technique in monitoring disease progression in a cohort of the interferon beta-1a (Rebif) treatment trial. J Neurol Neurosurg Psychiatry 2003;74(8)1090-1094.

44. Losseff NA, Webb SL, O'Riordan JI. Spinal cord atrophy and disability in multiple sclerosis. A new reproducible and sensitive MRI method with potential to monitor disease progression. Brain 1996;19(3):701-708.

45. Horsfield MA. Magnetization transfer imaging in multiple sclerosis.
J Neuroimaging 2005;15(4):58S-67S.

46. Barker GJ, Tofts PS, Gass A. An interleaved sequence for accurate and reproducible clinical measurement of magnetization transfer ratio. Magn Reson Imaging 1996;14(4):403-411.

47. Inglese M, Horsfield MA, Filippi M. Scan-rescan variation of measures derived from brain magnetization transfer ratio histograms obtained in healthy volunteers by use of a semi-interleaved magnetization transfer sequence. AJNR Am J Neuroradiol 2001;22(4):681-684.

48. Barbosa S, Blumhardt LD, Roberts N, Lock T, Edwards RHT. Magnetic resonance relaxation time mapping in multiple sclerosis – normal-appearing white matter and the invisible lesion load. Magn Reson Imaging 1994;12:33-42.

49. Neema M, Stankiewicz J, Arora A, et al. T1- and T2-based MRI measures of diffuse gray matter and white matter damage in patients with multiple sclerosis. J Neuroimaging 2007;17(Suppl 1)16S-21S.

50. Kidd D, Barker GJ, Tofts PS, et al. The transverse magnetisation decay characteristics of longstanding lesions and normal-appearing white matter in multiple sclerosis. J Neurol 1997; 244(2):125-130.

51. Butler JP, Reeds JA, Dawson SV. Estimating solutions of first kind integral equations with nonnegative constraints and optimal smoothing. SIAM J Numer Anal 1981;18(3):381-397.

52. Whittall KP, MacKay AL, Graeb DA, et al. In vivo measurement of T2 distributions and water contents in normal human brain. Magn Reson Med 1997;37(1):34-43.

53. Laule C, Kozlowski P, Leung E, et al. Myelin water imaging of multiple sclerosis at 7 T: correlations with histopathology. Neuroimage 2008 (in press).

54. Rovaris M, Gass A, Bammer R, et al. Diffusion MRI in multiple sclerosis. Neurology 2005;65(10):1526-1532.

55. Horsfield MA, Larsson HBW, Jones DK, et al. Diffusion magnetic resonance imaging in multiple sclerosis. J Neurol Neurosurg Psychiatry 1998;64(1): S80-S84.

56. Basser PJ, Mattiello J, LeBihan D. MR diffusion tensor spectroscopy and imaging. Biophys J 1994;66(1):259-267.

57. Turner R; LeBihan D, Maier J, et al. Echo-planar imaging of intravoxel incoherent motion. Radiology 1990;177(2):407-414.

58. Horsfield MA. Mapping eddy current induced fields for the correction of diffusion-weighted echo planar images. Magn Reson Imaging 1999;17(9):1335-1345.

59. Zhuang JC, Hrabe J, Kangarlu A, et al. Correction of eddy-current distortions in diffusion tensor images using the known directions and strengths of diffusion gradients. J Magn Reson Imaging 2006;24(5):1188-1193.

60. Andersson JLR, Skare S. A model-based method for retrospective correction of geometric distortions in diffusion-weighted EPI. Neuroimage 2002;16(1):177-199.

61. Mori S, Crain BJ, Chacko VP, et al. Three-dimensional tracking of axonal projections in the brain by magnetic resonance imaging. Ann Neurol 1999;45(2):265-269.

62. Jones DK, Travis AR, Eden G, et al. PASTA: Pointwise assessment of streamline tractography attributes. Magn Reson Med 2005;53(6)1462-1467.

63. Smith SM, Jenkinson M, Johansen-Berg H, et al. Tract-based spatial statistics:

Voxelwise analysis of multi-subject diffusion data. Neuroimage 2006;31(4):1487-1505.

64. Jones DK. Determining and visualizing uncertainty in estimates of fiber orientation from diffusion tensor MRI. Magn Reson Med 2003;49(1)7-12.

65. Pagani E, Filippi M, Rocca MA, Horsfield MA. A method for obtaining tract-specific diffusion tensor MRI measurements in the presence of disease: application to patients with clinically isolated syndromes suggestive of multiple sclerosis. Neuroimage 2005;26(1):258-265.

66. Tuch DS. Q-Ball imaging. Magn Reson Med 2004;52(6):1358-1372.

67. Tournier JD. Direct estimation of the fiber orientation density function from diffusion-weighted MRI data using spherical deconvolution. Neuroimage 2004;23(3):1176-1185.

68. Ostergaard L, Weisskoff RM, Chesler DA, et al. High resolution measurement of cerebral blood flow using intravascular tracer bolus passages. 1. Mathematical approach and statistical analysis. Magn Reson Med 1996;36(5):715-725.

69. Boxerman JL, Schmainda KM, Weisskoff RM. Relative cerebral blood volume maps corrected for contrast agent extravasation significantly correlate with glioma tumor grade, whereas uncorrected maps do not. AJNR Am J Neuroradiol 2006;27(4):859-867.

70. Gunther, M, Bock, M, Schad, LR. Arterial spin labeling in combination with a look-locker sampling strategy: Inflow turbo-sampling EPI-FAIR (ITS-FAIR). Magn Reson Med 2001;46(5):974-984.

71. Petersen ET, Zimine I, Ho YC, et al. Non-invasive measurement of perfusion: a critical review of arterial spin labelling techniques. Br J Radiol 2006;79(944):688-701.

72. Adhya S, Johnson G, Herbert J, et al. Pattern of hemodynamic impairment in multiple sclerosis: dynamic susceptibility contrast perfusion MR imaging at 3.0 T. Neuroimage 2006;33(4):1029-1035.

73**.** Rashid W, Parkes LM, Ingle GT, et al. Abnormalities of cerebral perfusion in multiple sclerosis. J Neurol Neurosurg Psychiatry 2004;75(9):1288-1293.

74. Inglese M, Adhya S, Johnson G, et al. Perfusion magnetic resonance imaging correlates of neuropsychological impairment in multiple sclerosis. J Cereb Blood Flow Metab 2008;28(1):164-171.

75. Zijdenbos AP, Forghani R, Evans AC. Automatic "pipeline" analysis of 3-D MRI data for clinical trials: application to multiple sclerosis. IEEE Trans Med Imaging 2002;21(10):1280-1291.

76. Liu LF, Meier D, Polgar-Turcsanyi M, et al. Multiple sclerosis medical image analysis and information management. J Neuroimaging 2005;15(4):103S-117S.

77. Xinapse Systems Limited, Jim image analysis software page. Available at: http://www.xinapse.com. Accessed March 10, 2008.

78. 3DSlicer. Available at: http://www.slicer.org. Accessed March 10, 2008.

79. Gering DT, Nabavi A, Kikinis R, et al. An integrated visualization system for surgical planning and guidance using image fusion and an open MR. J Magn Reson Imaging 2001;13(6):967-97.

80. U.S. Food and Drug Administration, Good Clinical Practice in FDA-Related Clinical Trials page. Available at: http://www.fda.gov/oc/gcp/. Accessed March 10, 2008.

81. The Association of Electrical and Medical Equipment Manufacturers, Digital Imaging and Communications in Medicine page. Available at: http://dicom.nema.org.

Accessed March 10, 2008.

Figure Legends

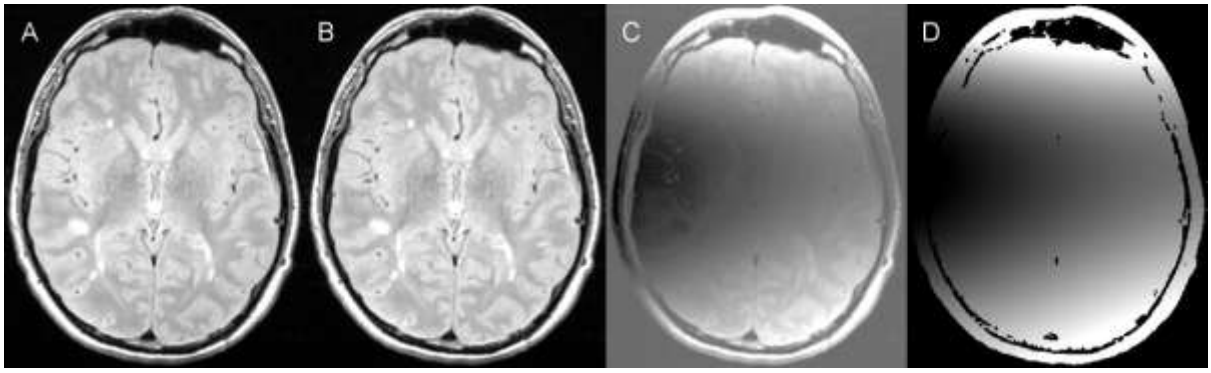

Figure 1. Bias field correction of a proton density image collected at 3 Tesla. (A) is the uncorrected image; (B) is has been non-uniformity corrected using the method in (6) that models the bias field using a 3-dimensional polynomial surface of order 3; (C) is the difference between (A) and (B); and (D) is a representation of the polynomial surface model of the bias field.

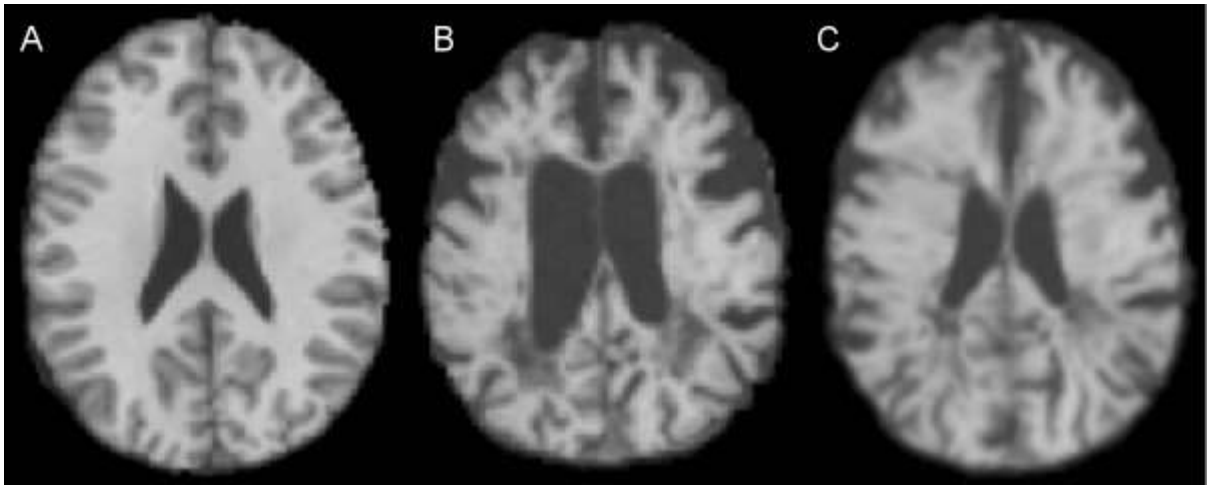

Figure 2. Linear (Affine) and non-linear registration. (A) is a normal control subject to which an MS patient with severe cerebral atrophy has been registered; (B) is the patient registered using an affine transform; (C) is the same patient but registered using the non-linear registration algorithm in Ref. 20. Illustration kindly provided by Dr. Elisabetta Pagani, Neuroimaging Research Unit, Ospedale S. Raffaele, University of Milan.

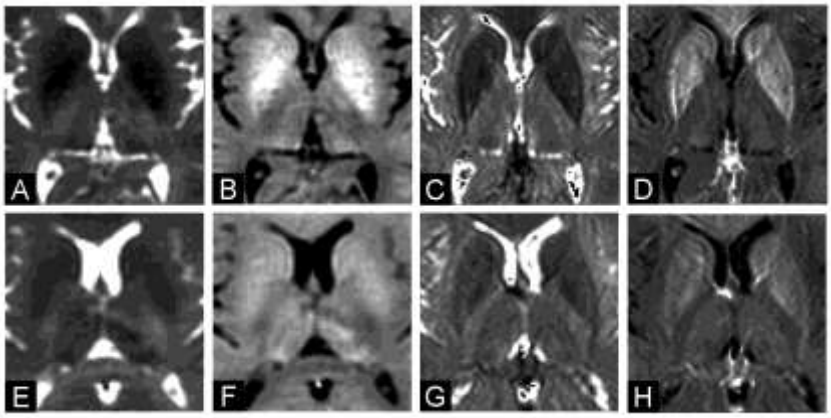

Figure 3. Relaxometry maps: T_2 (A, E), R_2 (B, F), T_2^* (C, G), and R_2^* (D, H) maps obtained at 3 Tesla are shown from a patient with relapsing–remitting multiple sclerosis (disease duration seven years, moderate disability [expanded disability status scale score 5]) (images A–D) and a healthy control (E–H). Marked hypointensity is seen in the caudate, putamen, and globus pallidus on T_2 and T_2^* maps from patient with MS (A, C) compared to the normal control (E, G). Similarly, marked hyperintensity is seen in the caudate, putamen and globus pallidus on R_2 and R_2^* maps from the patient with MS (B, D) compared to the normal control (F, H). The hypointensity seen on T_2 and T_2^* maps and hyperintensity seen on R_2 and R_2^* in the gray matter areas of patients with MS likely represents excessive iron deposition. *From* Neema M, Stankiewicz J, Arora A, et al. T_1- and T_2-based MRI measures of diffuse gray matter and white matter damage in patients with multiple sclerosis. J Neuroimaging 2007;17:16S-21S, with permission, Blackwell Publishing.

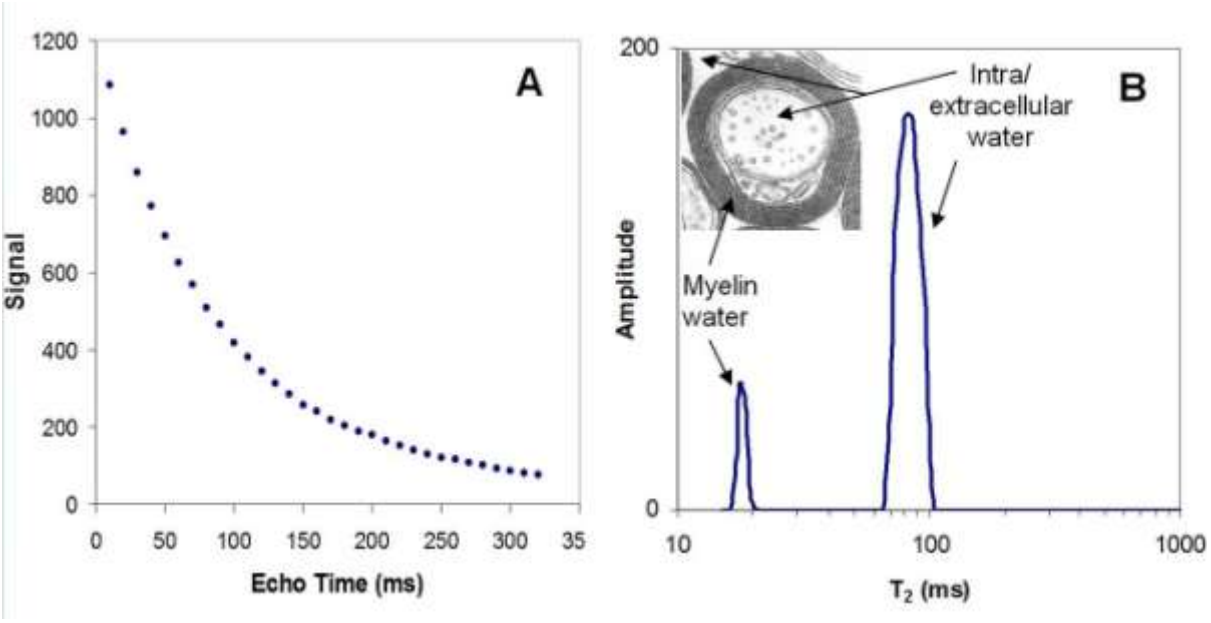

Figure 4. (A) T_2 decay curve and (B) T_2 distribution from human white matter. Inset in (B) shows a cross-section through an axon with the locations of the intra/extracellular water and myelin water. *From* Laule C, Vavasour IM, Kolind SH, et al. Magnetic resonance imaging of myelin. Neurotherapeutics 2007;4(3):460-84, with permission.

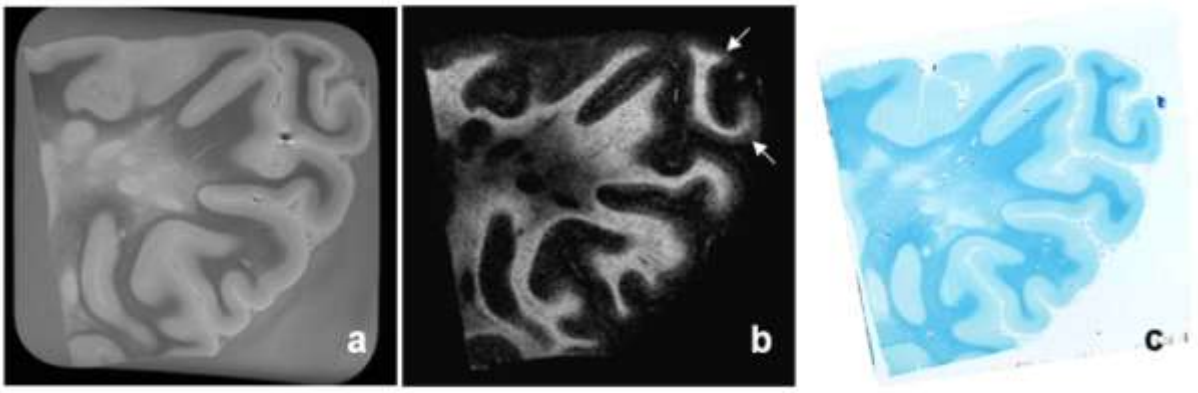

Figure 5. Formalin-fixed human brain tissue from the partieto-occipital lobe of an MS patient. MR images acquired at 7 Tesla: (a) short echo image image (TE=20.1 ms), and (b) myelin water map corresponding to that part of the T_2 distribution with values below 20 ms. (c) is the corresponding luxol fast blue histology image. A good qualitative correspondence is observed between the myelin water map and histology stain for myelin. The normal prominent myelination of the deeper cortical layers (arrows) is also visible on the myelin water image. *From* Laule C, Kozlowski P, Leung E, et al. Myelin water imaging of multiple sclerosis at 7 T: correlations with histopathology. Neuroimage 2008 (in press), with permission.

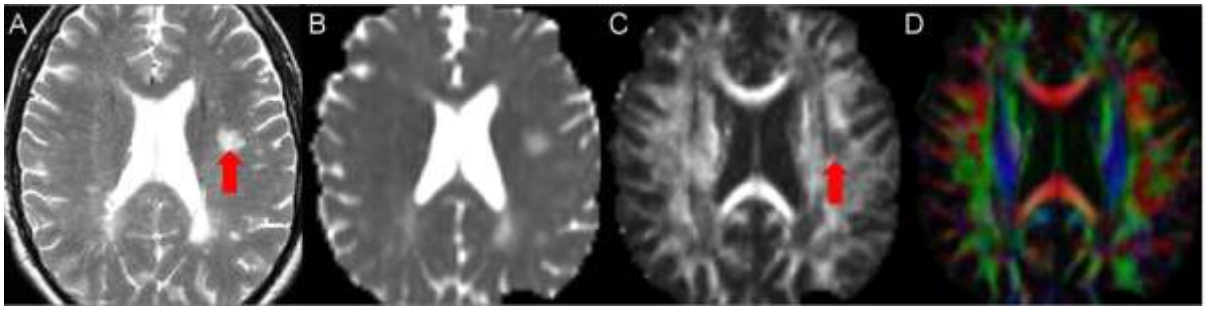

Figure 6. T_2-weighted image (A), diffusion tensor trace (B), fractional anisotropy (C) and color-coded direction maps (D) calculated from diffusion-weighted images of a patient with MS. Hyperintense lesions (such as the one arrowed) show high diffusivity and low anisotropy. In fiber-tracking applications (61), this causes greater uncertainty in the orientation of the axonal fibers, and tracking errors. In the direction map, axonal fibers which have a left-right orientation are colored red; anterior-superior are green; and superior-inferior are blue.

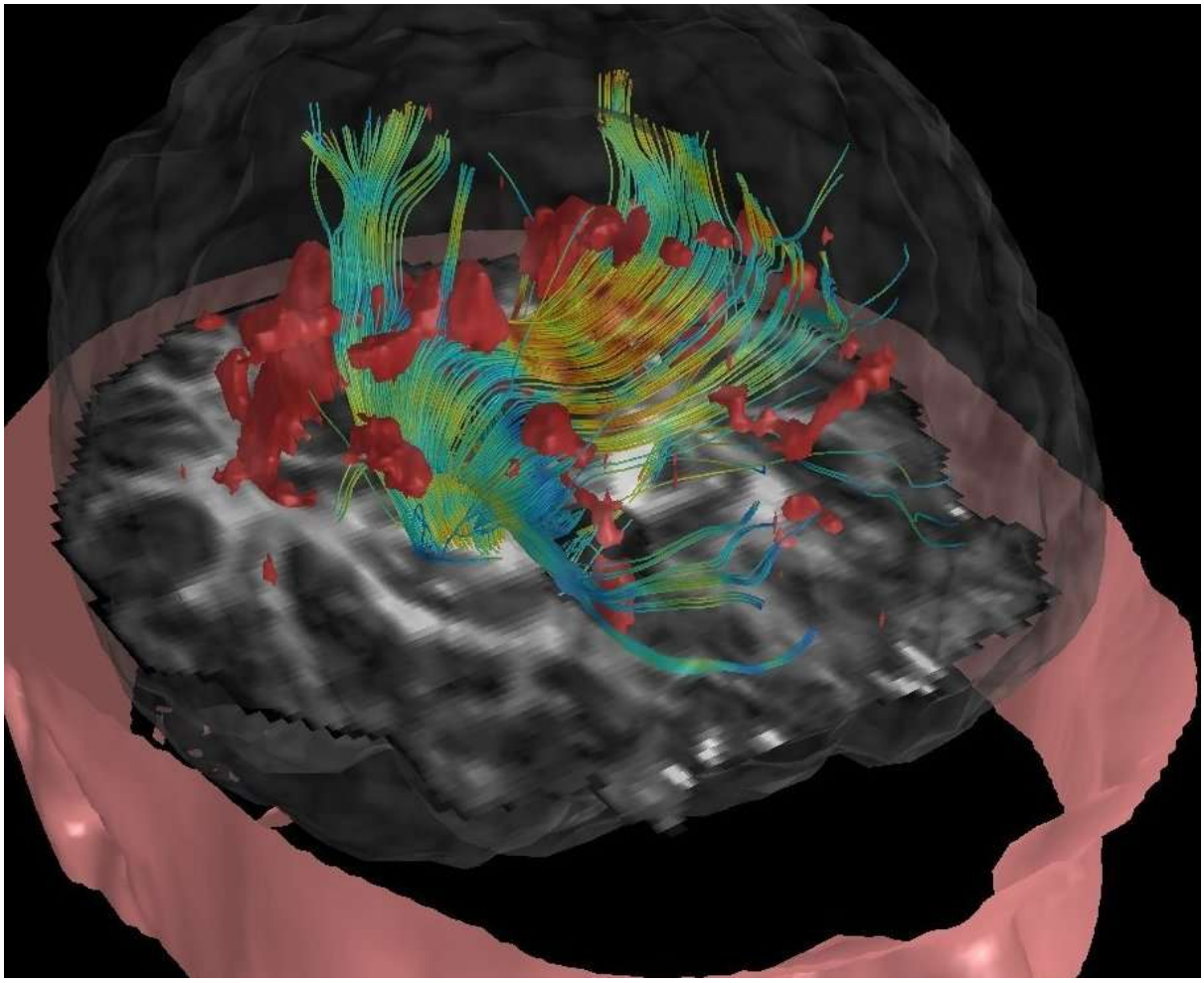

Figure 7. Tractography performed in a patient with MS. The MS lesions have been segmented from T_2-weighted images, and are rendered in red. Fiber tracking was initiated in the patient's right internal capsule, and the tracts pass through tissue affected by MS lesions. As they do so, the path spuriously deviates from the known motor tract and across corpus callosum.

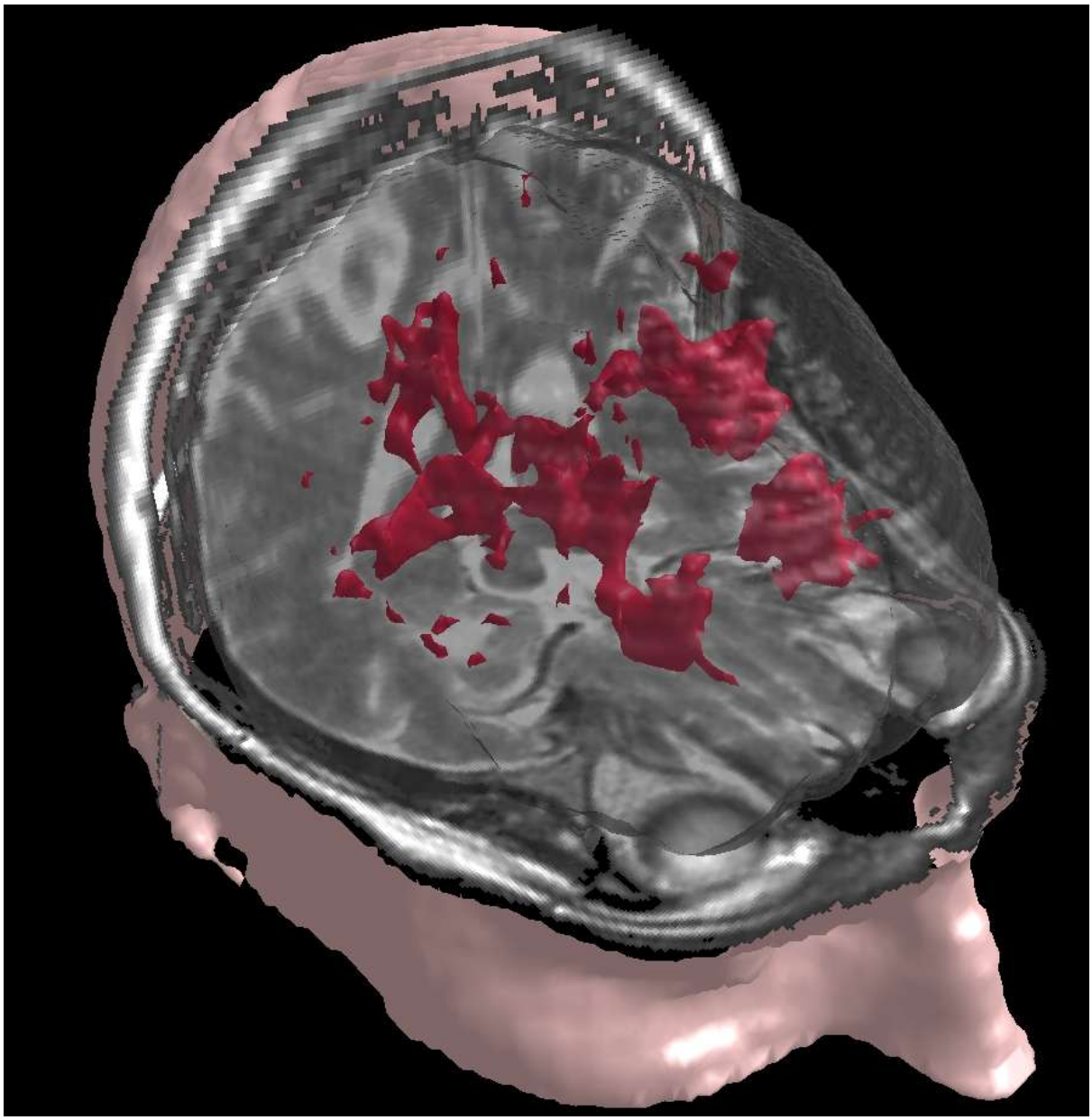

Figure 8. Graphic created using a three-dimensional visualization tool (77). The composite picture shows the surface-rendered skin surface in pink, a transparent extracted brain surface, MS lesions surface rendered in red, and a backdrop of orthogonal planes from a T_2-weighted image. The brain surface and lesions were found using pre-processing steps to automatically extract them (6,35).